Atmos. Meas. Tech., 12, 4733–4744, 2019
https://doi.org/10.5194/amt-12-4733-2019

Atmospheric Measurement Techniques
Open Access
EGU

Versatile aerosol concentration enrichment system (VACES) operating as a cloud condensation nuclei (CCN) concentrator: development and laboratory characterization

Carmen Dameto de España[1], Gerhard Steiner[1,2], Harald Schuh[1], Constantinos Sioutas[3], and Regina Hitzenberger[1]

[1]Department of Aerosol Physics and Environmental Physics, Faculty of Physics, University of Vienna, Vienna, 1090, Austria
[2]Institute for Ion Physics and Applied Physics, University of Innsbruck, Innsbruck, 6020, Austria
[3]Department of Civil and Environmental Engineering, University of Southern California, Los Angeles, CA 3620, USA

Correspondence: Carmen Dameto de España (carmen.dameto@univie.ac.at)

Received: 25 February 2019 – Discussion started: 19 March 2019
Revised: 15 July 2019 – Accepted: 16 July 2019 – Published: 5 September 2019

Abstract. The ability of atmospheric aerosol particles to act as cloud condensation nuclei (CCN) depends on many factors, including particle size, chemical composition and meteorological conditions. To expand our knowledge of CCN, it is essential to understand the factors leading to CCN activation. For this purpose, a versatile aerosol concentrator enrichment system (VACES) has been modified to select CCN at different supersaturations. The VACES enables sampling non-volatile CCN particles without altering their chemical and physical properties. The redesigned VACES enriches CCN particles by first passing the aerosol flow to a new saturator and then to a condenser. The activated particles are concentrated by an inertial virtual impactor and then can be returned to their original size by diffusion drying. For the calibration, the saturator temperature was fixed at 52 °C and the condenser temperature range was altered from 5 to 25 °C to obtain activation curves for NaCl particles of different sizes. Critical water vapour supersaturations can be calculated using the 50 % cut point of these curves. Calibration results have also shown that CCN concentrations can be enriched by a factor of approx. 17, which is in agreement with the experimentally determined enrichment factor of the original VACES. The advantage of the redesigned VACES over conventional CCN counters (both static and continuous flow instruments) lies in the substantial enrichment of activated CCN, which facilitates further chemical analysis.

1 Introduction

Atmospheric aerosols strongly influence the earth´s radiation balance directly by scattering and absorbing incoming short-wave radiation (direct effect) and indirectly by acting as cloud condensation nuclei (CCN). CCN particles can grow into cloud droplets (activate) at a critical water vapour supersaturation (Pruppacher and Klett, 2010). Increases in droplet number concentrations for the same water content can locally increase the albedo and the persistence of clouds (Abrecht, 1989). These are, respectively, termed the "Twomey" (first) and "cloud lifetime" (second) aerosol indirect effects (Twomey, 1977; Lohmann and Feichter, 2005; Charlson and Heintzenberg, 1995; IPCC, 2013). Cloud formation induced by the activation of atmospheric aerosols represents one of the main factors in determining the earth's radiative balance (Furutani et al., 2008) and consequently in estimating global climate change (IPCC, 2013; Houghton, 2001). To constrain these uncertainties and produce more accurate predictive models of the global climate system, it is essential to improve our understanding of the activation of aerosol particles to cloud droplets and the physicochemical properties of CCN (Furutani et al., 2008). The ability of an atmospheric aerosol particle to become a droplet depends on its size and chemical composition (Seinfeld and Pandis, 2006). Changes in aerosol size and composition during ageing increases a particle's susceptibility to CCN activation (Fierce et al., 2013). Numerous studies have been made in recent years for estimating the properties that enable particles to act as CCN (Burkart et al., 2011; McFiggans et al., 2006).

Particle size exerts the strongest influence on the ability of particles to act as CCN, since soluble mass changes with the third power of particle diameter (Andreae and Rosenfeld, 2008; Ervens et al., 2007). Chemical effects, however, can modify the ability of a particle to act as a CCN (Kreidenweis et al., 2006; Laaksonen et al., 1998). Insoluble but wettable particles can promote droplet formation. Hydrophilic substances strongly facilitate droplet activation, whereas hydrophobic substances can inhibit droplet formation (Andreae and Rosenfeld, 2008). According to Köhler theory, which describes the effects involved in cloud droplet activation, the critical supersaturation S_c is a function of a particle's chemical composition and size. This includes the number of potential solute molecules and their solubility (Tomasi et al., 2017). Compared to most soluble organic compounds, inorganic salts have a higher solubility, which results in a lower critical supersaturation for particles of equal size. Hings et al. (2008) showed that the S_c of 100 nm ammonium sulfate and adipic acid particles is 0.15 % and 0.27 %, respectively. The presence of slightly soluble aerosol material will further decrease the S_c (Kulmala et al., 1997; Zhang et al., 2012; Nenes et al., 2002). Organic compounds in particular can influence CCN activity via several mechanisms: contribution to solute matter, reduction of surface tension (e.g. Hitzenberger et al., 2002) and formation of hydrophobic surface films (Dusek et al., 2006; Kanakidou et al., 2005). The effects of organic compounds on CCN activation are still not well known. The large variety of atmospheric organic molecules and the numerous types of inorganic and organic aerosol material that are internally or externally mixed (e.g. Okada and Hitzenberger, 2001) further increase the difficulties in understanding CCN activity in the atmosphere. To gain more knowledge of atmospheric CCN, more characterization studies of CCN are needed. Numerous laboratory experiments have been carried out to explore the CCN activity of particles consisting of relatively simple model chemical species such as $(NH_4)_2SO_4$, NaCl and organic substances commonly detected in the atmosphere (e.g. Furutani et al., 2008; Giebl et al., 2002; Henning et al., 2005; Hings et al., 2008; Rose et al., 2008). As the number concentrations of CCN are quite low (mostly up to some 100 cm^{-3}), chemical analyses of activated CCN are quite challenging. To facilitate exploration of CCN properties, we therefore introduce an adapted concentration enrichment method to increase CCN concentrations for further analysis. The versatile aerosol concentration enrichment system (VACES) consists of an ambient particle concentrator developed by Sioutas et al. (1999). A VACES achieves enrichment of fine and ultrafine particles by first growing them to super-micron droplets in a supersaturation and condensation system and then concentrating them via a virtual impactor (Geller et al., 2005; Kim et al., 2001a; Wang et al., 2013a). These concentrated particles are enriched without being altered chemically or physically, except for the condensed water vapour, which can subsequently be removed by diffusion drying. In the case of particles containing semi-volatile or volatile species, some chemical changes may occur in the temperature range used in the VACES. The VACES has been used in a number of human and animal toxicological studies of the adverse effects of exposure to particulate matter (e.g. Klocke et al., 2017; Ljubimova et al., 2018; Wang et al., 2018). The VACES has been also used to measure particulate matter in different locations, such as in an underground railway station (Loxham et al., 2013), in Mexico City (De Vizcaya-Ruiz et al., 2006), in California's San Joaquin valley (Plummer et al., 2012) and in the Netherlands (Steenhof et al., 2011). Studies on emissions and exhaust particles from cars and their health effects were conducted with a VACES system by Tzamkiozis et al. (2010) and Gerlofs-Nijland et al. (2010). Other applications of the VACES included the determination of chemical properties of particulate matter sampled on filters (Verma et al., 2011; Wang et al., 2013c).

Modifications and further developments of the VACES for different applications were performed by e.g. Geller et al. (2005), Pakbin et al. (2011), Saarikoski et al. (2014), Wang et al. (2013b). Several recent studies corroborated the integrity of the VACES as a particle concentrator (e.g. Zhao et al., 2005; Ning et al., 2006; Ntziachristos et al., 2007; Saarikoski et al., 2014). Up until now, the VACES was operated at quite high water vapour supersaturations ratios (typically on the order of 1.5–1.8) to efficiently enrich ultrafine particles with sizes down to 10 nm. These high supersaturation ratios, however, are far too high to study CCN activation. In the atmosphere, typical supersaturations are much lower (around or below 0.5 %; Reade et al., 2006 and Aalto and Kulmala, 2000). For atmospheric CCN activation the chemical composition of particles is relevant in a limited size range between 30 and 200 nm (McFiggans et al., 2006). Particles smaller than 30 nm will hardly activate and particles larger than 200 nm are sufficiently large to activate practically irrespective of chemical composition. In our current study, we modified a VACES to operate at low supersaturations to enable enrichment of CCN. For the calibration runs, we used NaCl particles and polystyrene latex (PSL) particles with sizes in the range of 30 to 200 nm, i.e. the range where the chemical composition is relevant for particle activation at typical atmospheric supersaturations. We demonstrate the stability and reproducibility of this modified VACES for supersaturations < 0.6 %, which are far lower than the supersaturations used in the conventional VACES set-up. As an additional aspect, the concentration enrichment factor of the VACES' virtual impactors is measured in a novel way, i.e. from activation curves.

2 Theoretical background

Classical Köhler theory describes the equilibrium size of a droplet containing soluble material as a function of the water

Table 1. Parameters used to calculate the supersaturation for specific critical diameter and temperature (Weast, 1988).

Parameters	Values
Van 't Hoff factor NaCl	2
Density, NaCl (kg m^{-3})	2170
Density, water (kg m^{-3})	1000
Surface tension of water at 20 °C (N m^{-1})	0.072
Mw (kg mol^{-1})	0.018
Ms (kg mol^{-1})	0.059
Universal gas constant (J/(mol × K))	8.314

saturation ratio S and combines the Raoult and Kelvin effects. The Köhler equation is expressed by Eq. (1).

$$S = \frac{p}{p_0} = \left(1 + \frac{6 i m_\mathrm{s} M_\mathrm{w}}{M_\mathrm{s} \rho_w \pi d_\mathrm{d}^3}\right)^{-1} \exp\left(\frac{4\sigma_\mathrm{w} M_\mathrm{w}}{\rho_w R T d_\mathrm{d}}\right), \quad (1)$$

where S is defined as the actual vapour pressure p divided by the saturation vapour pressure p_0, i the van 't Hoff factor, m_s the mass of the solute, M_w and M_s the molecular masses of water and solute, respectively, R the universal gas constant, T the temperature in K, and ϱ_W and σ_w the density and the surface tension of water. d_d is the droplet size. This Köhler equation is difficult to solve analytically. For small supersaturations (i.e. S slightly above 1), a Taylor series expansion truncated after the first term can be used to obtain the critical supersaturation Sc ($Sc = S - 1$) and the critical droplet size $d_{\mathrm{d,c}}$ as follows (Seinfeld and Pandis, 2006):

$$S = \frac{p}{p_0} - 1 = \sqrt{\frac{256 \sigma_\mathrm{w}^3 M_\mathrm{w}^2 M_\mathrm{s}}{27 i R^3 T^3 \rho_w^2 \rho_S d_\mathrm{p}^3}}, \quad (2)$$

$$d_{\mathrm{d},c} = \sqrt{\frac{18 R T i m_\mathrm{s}}{4\pi \sigma_\mathrm{w} M_\mathrm{s}}}. \quad (3)$$

The activation and growth to droplet sizes of insoluble wettable particles is governed by the Kelvin effect (Hinds, 1999). The critical supersaturation for a spherical particle with a diameter d_p is given by the Kelvin equation (Eq. 4):

$$S = \frac{p}{p_0} - 1 = \exp\left(\frac{4\sigma_\mathrm{w} M_\mathrm{w}}{\rho_w R T d_\mathrm{p}}\right) - 1. \quad (4)$$

In this study, we use the parameters given in Table 1 to calculate critical supersaturations.

Critical supersaturations for particles of a given size and chemical composition can be measured from activation curves, where the activation ratio (defined as the ratio of the number concentrations of activated and unactivated particles) is plotted as a function of supersaturation. The 50 % point of this curve then gives the measured critical supersaturation for these particles. In the CCN-VACES, activation curves are obtained in a slightly different way by measuring the activation ratio as a function of the exit temperature T_out (see below). Knowing the temperature where 50 % of the particles activated and the particle size, the critical supersaturation can be calculated from Eq. (2).

3 Instrumentation

The new CCN-VACES is based on the previously developed VACES system (Kim et al., 2001a, b) and has numerous new features and modifications. The original VACES has two condenser tubes. In our set-up, both tubes are operated as prescribed, i.e. the aerosol flow passes both tubes, but the actual measurements are performed only at one of the tubes. The VACES operation principle has not been modified. This consists of first saturating the aerosol flow with water vapour and then cooling it down in the condenser to achieve supersaturation, particle activation and growth by water condensation. The grown particles are concentrated in the minor flow of the virtual impactor, while particles smaller than the cut size of the virtual impactor are removed from the system in the major flow. From the original VACES, only the virtual impactors and the temperature regulator and chiller for the condenser tubes were used, while the saturator and condenser parts were changed (see below) in the CCN-VACES.

3.1 Saturator

A new vertical heat-insulated stainless steel cylinder tank that is 40 cm long, 40 cm in diameter and partially filled with ultrapure water (Direct-Q5®, Millipore, Billerica, MA) is placed on two 18 cm diameter electric hotplates (1500 W, EKP3582, Clatronic®), which are switched on and off with a solid-state relay controlled by an Arduino microcontroller board (ARDUINO® is an open-source platform that consists of both hardware and software to be used for process control) to keep the water temperature constant within 0.2 °C. A small water pump inside the tank keeps the water well mixed and ensures a homogeneous temperature profile within the water tank. Temperature sensors measure the water temperature T_w and the air temperature inside the saturator vessel directly before the aerosol outlet (saturator temperature T_s). Aerosol is introduced into the space above the heated water where it is saturated with water vapour and subsequently led into the cooling tubes of the VACES. In these cooling tubes, the water vapour becomes supersaturated and condenses on the particles. The total flow rate of the system is determined by the flow rate of the virtual impactor (105 L min^{-1}), so the test aerosol used here (monodispersed NaCl aerosol produced with a DMA with an aerosol flow rate of 5 L min^{-1}; see below) had to be diluted with ambient filtered air to achieve the necessary volume flow. The duct between the saturator outlet and the inlet of the cooling tube used here is heated by a heat-

ing wire to the saturator temperature and fitted with thermal insulation to prevent premature water condensation.

3.2 Condenser

The water-vapour-saturated air is drawn into two parallel 1 m long steel tubes each consisting of a 2.2 cm diameter inner tube surrounded by a 7.62 cm diameter outer tube. The space between the two concentric tubes is filled with an ethylene glycol and water (1 : 1 by volume) coolant. The outer tube is connected at the beginning and at the end of the tube with a commercially available recirculating chiller (Thermocube 300 1D 1 LT Solid State Cooling Systems, Pleasant Valley, NY), which regulates the coolant temperature within $\pm 0.1\,^{\circ}\mathrm{C}$. The coolant temperature in the tube is defined here as condenser temperature T_c. In order to preserve the preset temperature, both condenser tubes are insulated with polyethylene foam pipes. In these condenser tubes the warm saturated air exiting the saturator is cooled below the dew point to achieve supersaturation, so aerosol particles can activate and grow to droplets with sizes of about 2.5–3 µm (Daher et al., 2011; Kim et al., 2001a). At the exit of the condenser, the air temperature T_{out} is measured.

3.3 Virtual impactor

The two condenser tubes are each followed by a virtual impactor with a nominal cut point of 1.5 µm. Virtual impactors classify particles according to their inertia by separating them into two streams according to their aerodynamic diameters (e.g. Marple and Chien, 1980). The aerosol passes first through an accelerating nozzle and is directed to a collection probe where the size classification occurs. At this point a major part of the flow is diverted 90° away from the collection probe. Particles with a smaller aerodynamic diameter and lower inertia follow the streamlines of the major flow, while particles with aerodynamic diameters larger than the cut size continue moving axially in their forward path, penetrating further into the collection probe with the minor flow (Kulkarni et al., 2011). The separation efficiency curve is determined by the ratio of the major and minor flows and the physical dimensions of the nozzle and collection probe. Besides the particle-size separation, the virtual impactor concentrates particles larger than its cut size in the minor flow. The theoretical enrichment factor is equal to the ratio of the total flow rate to the minor flow rate. One characteristic of a virtual impactor is that particles smaller than the cut size of the impactor remain in the both major and minor flows. As the minor flow in our case is 5 % of the total flow, only 5 % of the small particles will remain with the minor flow. The construction of a virtual impactor has a strong influence on the shape of the separation efficiency curve and on particle losses (Marple and Chien, 1980). The characterization of virtual impactors and their collection efficiency curves has been intensively studied by Sioutas et al. (1994, 1999) and Sioutas and Koutrakis (1996). The virtual impactors used in our study are identical to those used by Kim et al. (2001a) with a major flow of 105 and a minor flow of $5\,\mathrm{L\,min^{-1}}$. In our set-up, the minor flow exiting the virtual impactor is passed through a diffusion dryer and then split into two flows. One flow ($0.6\,\mathrm{L\,min^{-1}}$) is led to a condensation particle counter (CPC; Grimm 5412, flow rate $0.6\,\mathrm{L\,min^{-1}}$), while the other flow ($4.4\,\mathrm{L\,min^{-1}}$, regulated with a flow controller) is vented to the exhaust. The collection efficiency curves and particle losses of the virtual impactor used here were calculated by Sioutas et al. (1994). The theoretical concentration enrichment factor $\mathrm{EF_{Theo}}$ is given by Eq. (5).

$$\mathrm{EF_{Theo}} = \frac{Q_{\mathrm{tot}}}{q_{\mathrm{min}}} (1 - \mathrm{WL})\, \eta_{vi}, \tag{5}$$

where Q_{tot} and q_{min} are the total and minor flows of the impactor, respectively, and WL and η_{vi} are the fractional losses and the collection efficiency, respectively (Sioutas et al., 1999). For a VACES, small values of WL and the assumption that the virtual impactor collection efficiency η_{vi} at 50 % droplet activation is around 1, the enrichment factor approaches the theoretical enrichment factor given by Eq. (6).

$$\mathrm{EF_{Theo}} = \frac{Q_{\mathrm{tot}}}{q_{\mathrm{min}}} \tag{6}$$

3.4 Monodisperse aerosol generation

NaCl particles were generated by nebulizing a $10\,\mathrm{g\,L^{-1}}$ solution of sodium chloride (Applichem GmbH, $> 99\,\%$) in ultrapure water with a Collison atomizer (TSI, 3076) operated with particle-free air at 1.2 bar, producing a $2\,\mathrm{L\,min^{-1}}$ flow. This flow was diluted with $3\,\mathrm{L\,min^{-1}}$ of dry clean air and dried to relative humidities $< 15\,\%$ with a diffusion dryer. The $5\,\mathrm{L\,min^{-1}}$ total flow was neutralized with a soft X-ray charger (TSI, 3087) to bring the aerosol into charge equilibrium. A Vienna-type differential mobility particle sizer (DMPS) (Winklmayr et al., 1991) was operated in a closed loop arrangement and used to generate monodisperse particles with sizes of 30, 100, 150 and 200 nm mobility equivalent diameter. The size selective behaviour of the DMA was tested with monodisperse PSL particles (Polyscience Inc. Warrington, PA) of various sizes. Before each measurement run all flow rates were checked with a Gilibrator high-flow generator cell (Sensidyne™, 800265). PSL particles with sizes of 100 and 150 nm were used to check the CCN-VACES calibration for insoluble particles.

3.5 Experimental set-up

The CCN-VACES was evaluated measuring the enriched particle number concentration at different temperature settings of the saturator and condenser. For these measurements, monodisperse NaCl aerosol was drawn through the saturated water vapour atmosphere in the heated water tank before entering the cooling sections (condenser tubes) of the VACES.

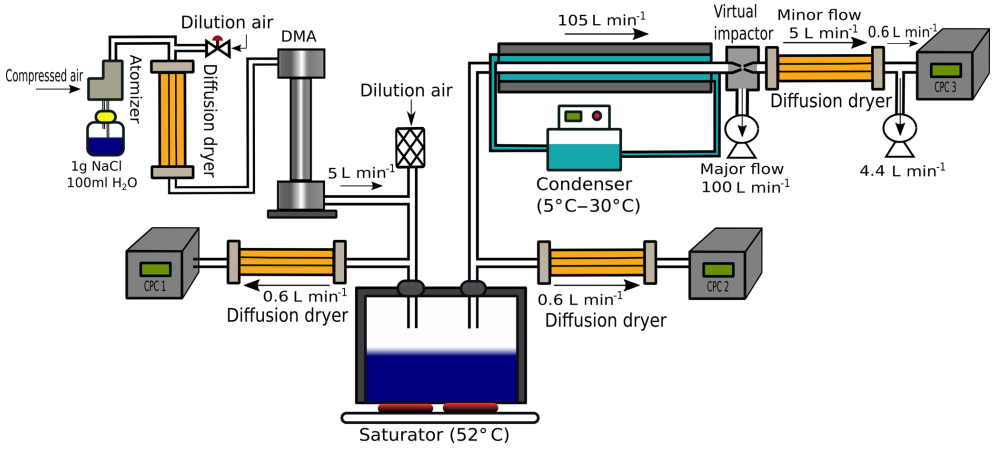

Figure 1. Set-up for the CCN-VACES calibration. Only one condenser tube is used for the calibration.

In order to have an incoming particle number concentration reference, the particle number concentration was measured before entering the saturator tank with the first CPC (Grimm 5412; flow rate 0.6 L min^{-1}), which corresponds to CPC 1 in Fig. (1). Tank water temperature, T_w, was set at 52 °C and kept constant within 0.2 °C. Before starting the measurements the water level in the tank was checked to ensure a water volume of 24 L. Water heating time was around 1 h, followed by a stabilization time of 30 min to achieve a constant water temperature. As the system is very sensitive to temperature variations, keeping the water temperature constant was very important. The aerosol residence time in the tank was about 8 s to ensure saturation of the aerosol stream. Although the saturated aerosol is drawn through both tubes in parallel, only one tube was used in the following experiments. Prior to entering the condenser tube, the inlet particle number concentration was measured with a isokinetic sampling tube (8 mm diameter) connected to a diffusion dryer to remove excess humidity, followed by a second CPC (Grimm 5412; flow rate 0.6 L min^{-1}, referred to as CPC 2 in Fig. 1). This number concentration is defined as the inlet concentration C_{in}. After passing through the condenser tube, the aerosol is separated into two size classes by the virtual impactor (nominal cut size 1.5 µm aerodynamic diameter). The minor flow from the virtual impactor containing the activated droplets is connected to a diffusion dryer to dry the droplets to their original size. A third CPC (Grimm 5412; flow rate 0.6 L min^{-1}; referred to as CPC 3 in Fig. 1) was used to measure the number concentration of the enriched particles. Before each calibration run, the system was checked for leaks and all flow rates were measured. The output concentration of the atomizer was checked for fluctuations, as these fluctuations are indicators of leaks or impurities in the system. Measurements were started after T_w was found to be stable (see above). For the calibration curve measurements, the aerosol was passed through a DMA to select a particle size, led through the saturator tank and subsequently into the condenser, which was set to a fixed temperature. At the start of a calibration run, T_c was set at 30 °C followed by 25 °C. At these two temperatures no noticeable changes in the condenser outlet concentration were observed. T_c was subsequently reduced in 1 °C increments. At each temperature setting, ca. 20 min were necessary for the system to stabilize. Inlet concentration, outlet concentration, T_w, T_s, T_c, T_{out} and laboratory temperature were recorded after stabilization for 5 min with a time resolution of 1 s to ensure good statistical results. Each data point in Figs. 3–6 therefore corresponds to the mean value of 300 individual measurement points The time required for an activation curve measurement was 6 to 8 h.

4 Results and discussion

4.1 Measurement of the enrichment factor of the CCN-VACES set-up

The CCN-VACES was tested first by determining the experimental concentration enrichment factor using NaCl and PSL particles of different sizes. PSL particles were used to check whether the CCN-VACES operates well also for non-hygroscopic aerosols. For the measurements T_w was set at 52 °C (±0.2 °C) and T_c was varied from 20 to 5 °C with steps of 1 °C (±0.1 °C). The concentration of the minor flow is enriched by a factor that ideally is equal to the ratio of total sample flow rate to the minor flow rate (Kim et al., 2001a). In order to determine the experimental enrichment factor of our modified set-up, activation curves were used in which the ratio of the outlet concentration to the inlet concentration is plotted over the temperature difference ΔT between the saturator temperature T_s and the condenser temperature T_c. In the measurements of enrichment factors, ΔT was used as independent variable in order to make our results comparable to previously published enrichment factors, which investigated the enrichment factor in terms of T_c. The experimental en-

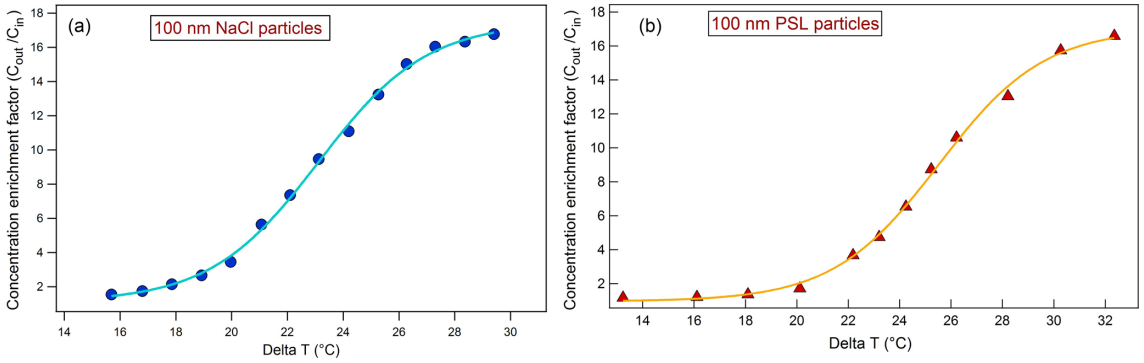

Figure 2. (a) Experimentally determined concentration enrichment factor for 100 nm NaCl particles at different ΔT (difference between the saturator temperature T_s and the condenser temperature T_c). **(b)** Experimentally determined concentration enrichment factor for 100 nm PSL particles as a function of ΔT. The maximum experimental enrichment factors correspond to 100 % activation.

richment factor curves obtained for 100 nm NaCl and PSL particles are shown in Fig. (2).

The maximum experimental enrichment factor obtained for different particle sizes is given in Table 2. These experimental enrichment factors (EF_{Exp}) can be compared with the theoretical enrichment factor (EF_{Theo}) calculated according to Eq. (6). A total flow of 105 L min^{-1} and a minor flow of 5 L min^{-1} result in an $EF_{Theo} = 21$. The experimental enrichment factor corresponds to around 80 % of the theoretical enrichment factors, which corroborates the efficiency of 80 % of the original VACES set-up (Kim et al., 2001b). These results can be compared with other already published studies. In the study by Geller et al. (2005), the enrichment factor for 50 and 170 nm PSL particles was found to be 15 and 15.3, respectively. The theoretical enrichment factor in the study by Geller et al. (2005) is 20, so the experimental enrichment factor corresponds to 75 % of the theoretical enrichment factor. These results agree with our experimental enrichment factor results.

4.2 Size dependence of the activation curves

The CCN-VACES was calibrated using the set-up given in Fig. (1) from activation curves obtained for monodispersed particles of known chemical composition (e.g. Rose et al., 2008; Dusek et al., 2006). One important issue in this study was to analyse the dependence of the activation of particles of different sizes on the temperature settings. For this experiment, T_w was again set at 52 °C (±0.2 °C) and T_c was again decreased from 20 to 5 °C (±0.1 °C) in steps of 1 °C. The actual temperature at the exit of the condenser (T_{out}) determines the supersaturation experienced by the particles. This temperature, however, cannot be set, so in this part of the study, we set T_c and used the particles of different sizes as "supersaturation sensors". Different activation curves were measured for different particle sizes. Normally, the activation ratio of an aerosol is defined as the concentration of the activated divided by the total particle concentration. In our case, the enrichment factor of the virtual impactor has to be taken into account, so here (Fig. 3) the activation ratio is given as $(C_{out}/C_{in})/(C_{out}/C_{in})_{max}$ where $(C_{out}/C_{in})_{max}$ is essentially the measured enrichment factor given in Table 2, so the activation curves are normalized to 1 at 100 % activation. Figure 3 shows the normalized activation curves for particles of different size as a function of the temperature difference between T_s and T_c (ΔT). The error bars corresponding to the standard error of the mean are included.

Based on Köhler theory, the critical supersaturation is a function of $T^{-3/2}$ and $d_p^{-3/2}$ which translates into higher critical supersaturations for small particle activation compared to activation of larger particles. These higher critical supersaturations are achieved by larger ΔT or, at fixed saturator temperatures T_s, lower condenser temperatures T_c. Larger particles activate at lower critical supersaturations and, in our case, smaller ΔT (i.e. higher T_c). This behaviour can be observed in Fig. 3. The activation curve for 30 nm particles is shifted to the right (larger ΔT) compared to the curve for 200 nm particles.

4.3 Reproducibility

The reproducibility of activation curves measured with the CCN-VACES was also tested. Different calibration curves were measured on different days using the same temperature settings. By comparing results from the same particle size and temperature settings, we obtained identical activation curves, which demonstrates that the CCN-VACES is reliable as a particle activator. Figure 4 shows an example of activation curves obtained for 100 nm NaCl particles on different days but at the same laboratory temperature $T_{Lab} =$ 23 °C. The data points coincide on the same fitted curve. Further results also demonstrate that the activation curves do not depend on the inlet concentration. Curves obtained for monodisperse particles with a 6000 cm^{-3} concentration were found to be identical to curves obtained for particles of the same size and with a concentration of 2000 cm^{-3}. This find-

Table 2. Comparison between the measured experimental enrichment factors for NaCl and PSL particles with different sizes to the calculated theoretical enrichment factor. The measured enrichment factor corresponds to roughly 80 % of the theoretical enrichment factor, which agrees with the VACES efficiency given by Kim et al. (2001b). The measured enrichment factors do not depend on particle size and type.

Particle size	Experimental concentration enrichment factor EF_{Exp}	Theoretical concentration enrichment factor EF_{Theo}	Enrichment efficiency ratio (experimental/theoretical)
NaCl			
30 nm	16.6	21	79 %
100 nm	16.4	21	78 %
150 nm	17.0	21	81 %
200 nm	16.8	21	80 %
PSL			
100 nm	16.59	21	79 %
150 nm	16.12	21	77 %

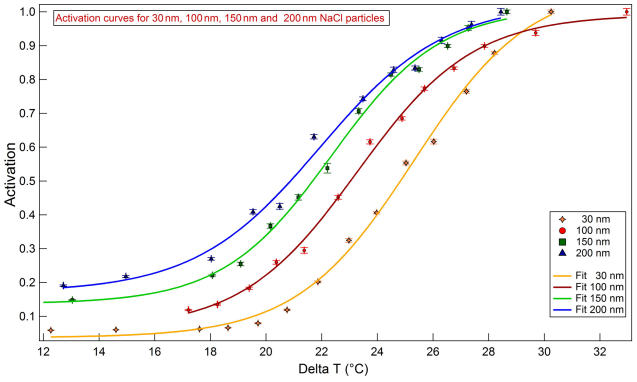

Figure 3. Activation curves for NaCl particles of different sizes at different ΔT, which is the temperature difference between the saturator temperature T_s and condenser temperature T_c. The measured values (points) are fitted with sigmoidal curves.

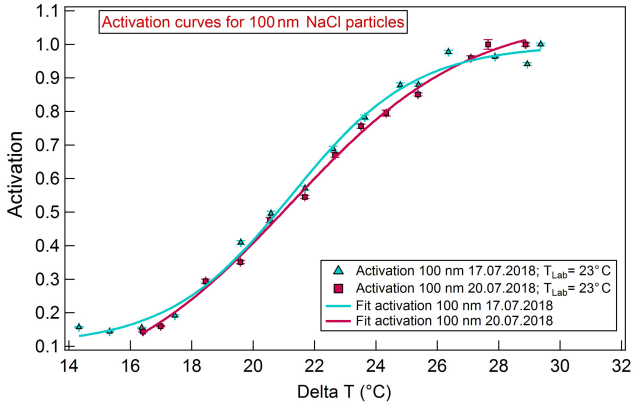

Figure 4. Activation curves for 100 nm NaCl particles measured on two different days. Both curves are equivalent.

ing agrees with previous studies by Sioutas and Koutrakis (1996).

Dependence on ambient temperature

When measuring the activation curves, the CCN-VACES system was found to be extremely sensitive to slight variations in the temperature settings. In addition, ambient (laboratory) temperature was found to have a noticeable effect on the saturator temperature T_s. In order to obtain identical activation curves for particles of a certain size, the ambient temperature also has to remain fairly constant. As the CCN-VACES draws 205 L min^{-1} filtered ambient air, the temperature of the aerosol stream inside the system is influenced by the ambient temperature, which has an effect on the supersaturation achieved in the condenser. This behaviour was seen by comparing activation curves as function of ΔT obtained in different seasons, with different laboratory temperatures (in summer this is around 27 °C and in winter it is 22 °C). As there is no way to set the temperature of the aerosol stream at the outlet of the saturator (i.e. T_s), the only temperature that can be controlled in the saturator is the water temperature T_w. For the experiments shown in Fig. 5, the water temperature was always set to $T_w = 52$ °C. Mixing of the aerosol stream with filtered ambient air resulted in a saturator temperature $T_s = 39$ °C in summer and $T_s = 37.5$ °C in winter. This saturator temperature difference has a strong influence on the outlet temperature measured T_{out} at the exit of the condenser and consequently on the actual supersaturation experienced by the particles. As a result, the activation curves measured during summer are shifted to the left (red curve in Fig. 5) compared to the activation curve measured in winter (blue curve in Fig. 5) for the same setting of ΔT.

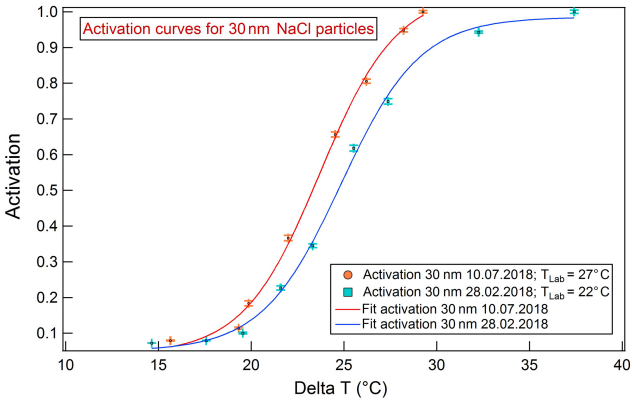

Figure 5. Activation curves for NaCl particles with 30 nm size measured in winter (blue curve, laboratory temperature 22 °C) and summer (red curve, laboratory temperature 27 °C).

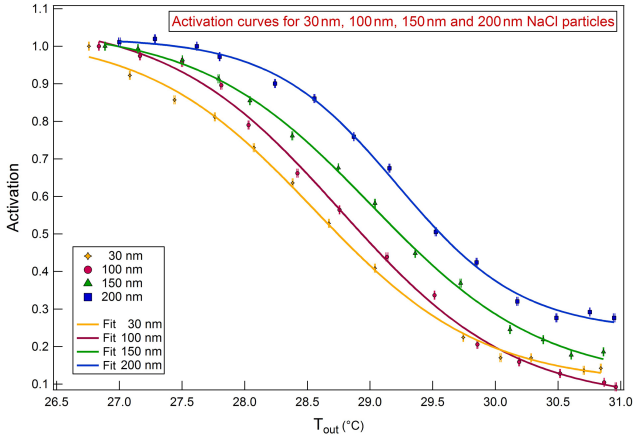

Figure 6. Activation curves as a function of T_{out} (measured between the condenser tube and the virtual impactor) for NaCl particles of different sizes. Measured points fitted with sigmoidal curves.

4.4 Determination of the supersaturation in the CCN-VACES

In order to determine the supersaturation experienced by the particles downstream of the condenser tube, a temperature sensor was inserted in the connector between the condenser and the virtual impactor. As the flow is turbulent, the temperature sensor was put at the inner surface of the (thermally insulated) connector. This temperature is referred to here as T_{out} and corresponds to the temperature of the particles right before they enter the virtual impactor. For the calculation of the actual supersaturations achieved in the condenser, activation curves are plotted as a function of T_{out}. T_{out} at the 50 % point of the curves was used to obtain S_C from Eq. (2) for NaCl particles and Eq. (4) for PSL particles. In the following Fig. 6, activation curves of NaCl particles are shown with the corresponding error bars. In Fig. 6 the activation curves have a smooth slope, which agrees with results obtained in other studies, such as Giebl et al. (2002) or Frank et al. (2007). For the determination of the critical supersaturation, a sigmoidal curve was fitted to each data set. As the supersaturation is proportional to $T^{-3/2}$, smaller particles activate at higher supersaturations and therefore at lower temperature T_{out}. The curve for 200 nm particles shows that 30 % of the particles are already activated at $T_{out} = 31$ °C. For 100 nm particles, this fraction is 10 %. In contrast to Fig. 3, where the activation curve for 30 nm particles is shifted to the right, in Fig. 6 the activation curve for 30 nm particles is shifted to the left. This is due to the different presentation: in Fig. 3 the activation ratio is plotted as a function of ΔT and in Fig. 6 as a function of T_{out}. The curves also show that activation is extremely sensitive to T_{out}. The difference in T_{out} from one activation curve to the next in Fig. 7 is only 0.2 °C. For 30 nm particles, T_{out} at 50 % activation is 28.6 °C, whereas for 100 nm NaCl particles it is 28.8 °C. As shown in Fig. 7a–d, the temperature at which 50 % of the particles activate can be obtained. Based on this temperature, the supersaturation can be determined from Eq. (2) using the values of the parameters given in Table 1. Results of the corresponding temperature together with the calculated supersaturation are given in Table 3. The critical supersaturation for PSL particles was calculated from Kelvin theory (Eq. 4). As PSL particles are insoluble the critical supersaturation only depends on the Kelvin term previously defined in the Sect. 2. The results presented in Table 3 show that PSL particles need higher critical supersaturations to activate than NaCl particles of comparable size. For example, 100 nm PSL particles need a critical supersaturation of 2.1 %, whereas 100 nm NaCl particles activate at 0.1 % critical supersaturation. These results are in agreement with Köhler theory: the more hygroscopic the particles the lower the supersaturation needed to activate them.

Table 3. Calculated critical supersaturations at the measured T_{out} (at 50 % activation) for NaCl and PSL particles of different sizes.

Particle size (nm)	T_{out} for 50 % activation (K)	S_{crit} (%)
NaCl		
200	302.37	0.035 %
150	302.16	0.054 %
100	301.92	0.099 %
30	301.71	0.602 %
PSL		
100	299.03	2.107 %
150	300.35	1.394 %

5 Summary and conclusions

In this work we have shown that the overall performance of the CCN-VACES is similar to that of the original VACES.

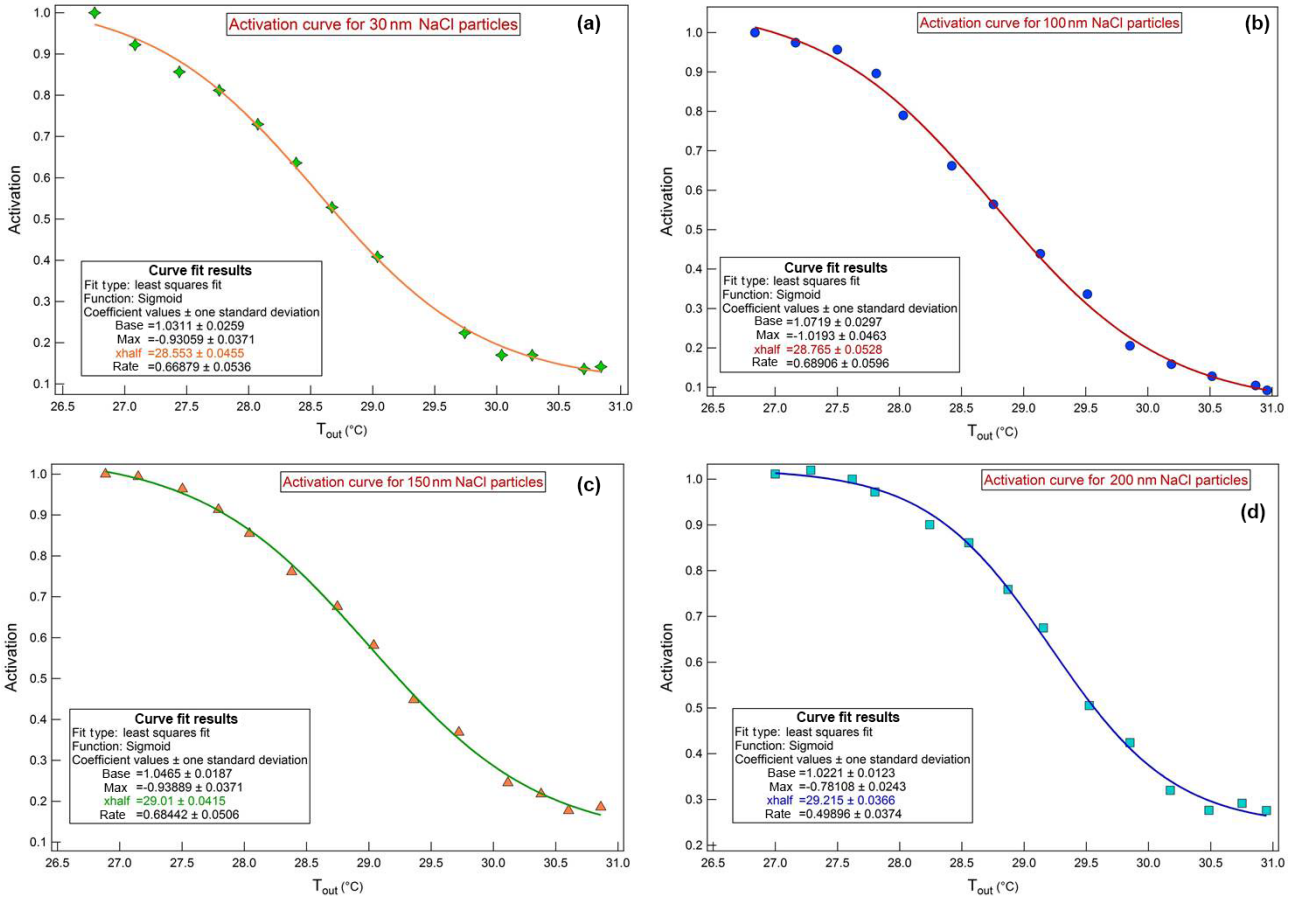

Figure 7. Determination of the critical supersaturation for four different activation curves.

Our experimentally determined enrichment factor was about 16.5–17.0, which is somewhat lower than the theoretical enrichment factor of 21 but similar to values obtained in other studies for the original VACES (Wang et al., 2016). Our results show that the CCN-VACES is reliable as a particle activator and can enrich CCN at low supersaturations ($< 0.6\,\%$). It is, however, dependent on ambient conditions and very sensitive to the temperature settings. To measure activation curves for particles of different sizes, the temperature settings have to remain as stable as possible. The water temperature T_w and the saturator temperature T_s variations during a measurement series should be less than 1 °C. In this study, we used the temperature at the exit of the condenser (i.e. T_{out}), where 50 % of the particles activate, and the known dry particle size to calculate the supersaturation. We observed that for 100 nm NaCl particles, this temperature was 28.8 °C, while for 30 nm NaCl particles it was 28.6 °C. The difference between these two temperatures is only 0.2 °C, whereas the corresponding particle size difference is 70 nm. If the CCN-VACES is used as a CCN concentrator, calibration runs should be performed for each supersaturation setting with test particles of sufficiently different size. Notwithstanding the strong temperature dependence, we found that the CCN-VACES is a reliable instrument to activate CCN and enrich CCN concentrations at low supersaturations, provided that the temperature settings are carefully controlled. Some changes in particles containing volatile or semi-volatile substances, however, might occur in the temperature range used in the saturator and condenser. In contrast to continuous-flow CCN counters (Rose et al., 2008) and static-thermal-gradient CCN counters (Giebl et al., 2002), the CCN-VACES provides enriched CCN concentrations for further analysis.

Data availability. Data can be accessed by contacting the corresponding author.

Author contributions. CD designed and developed the modified VACES and contributed to the experiments, data analysis and MS preparation. GS designed the experiment, prepared the experimental set-up and interpreted the data. HS designed and performed the technical development of the experiment. CS developed the VACES system and provided technical support for the preparation of the manuscript. RH initiated and supervised this research work and provided advice on the experiment and data analysis and extensive input towards the text of the manuscript.

Competing interests. The authors declare that they have no conflict of interest.

Acknowledgements. The authors wish to thank Anna Wonaschütz and Christoph Hitzenberger for helpful discussions and Christian Tauber for providing the data acquisition programme for the simultaneous recording of particle concentrations and temperature settings. Open-access funding provided by University of Vienna.

Review statement. This paper was edited by Johannes Schneider and reviewed by two anonymous referees.

References

Aalto, P. and Kulmala, M.: Using a cloud condensation nuclei counter to study CCN properties and concentrations, Boreal Environ. Res., 7, 349–359, 2000.

Abrecht, B. A.: Aerosols, Cloud Microphysics, and Fractional Cloudiness, Science, 245, 1227–1230, https://doi.org/10.1126/science.245.4923.1227, 1989.

Andreae, M. O. and Rosenfeld, D.: Aerosol-cloud-precipitation interactions. Part 1. The nature and sources of cloud-active aerosols, Earth-Sci. Rev., 89, 13–41, https://doi.org/10.1016/j.earscirev.2008.03.001, 2008.

Burkart, J., Steiner, G., Reischl, G., and Hitzenberger, R.: Long-term study of cloud condensation nuclei (CCN) activation of the atmospheric aerosol in Vienna, Atmos. Environ., 45, 5751–5759, https://doi.org/10.1016/j.atmosenv.2011.07.022, 2011.

Charlson, R. J. and Heintzenberg, J. J.: Aerosol forcing of climate: report of the Dahlem Workshop on Aerosol Forcing of Climate, Berlin 1994, 24–29 April, J. Wiley, 1995.

Daher, N., Ning, Z., Cho, A. K., Shafer, M., Schauer, J. J., and Sioutas, C.: Comparison of the Chemical and Oxidative Characteristics of Particulate Matter (PM) Collected by Different Methods : Filters, Impactors, and BioSamplers, 37–41, https://doi.org/10.1080/02786826.2011.590554, 2011.

De Vizcaya-Ruiz, A., Gutiérrez-Castillo, M. E., Uribe-Ramirez, M., Cebrián, M. E., Mugica-Alvarez, V., Sepúlveda, J., Rosas, I., Salinas, E., Garcia-Cuéllar, C., Martínez, F., Alfaro-Moreno, E., Torres-Flores, V., Osornio-Vargas, A., Sioutas, C., Fine, P. M., Singh, M., Geller, M. D., Kuhn, T., Miguel, A. H., Eiguren-Fernandez, A., Schiestl, R. H., Reliene, R., and Froines, J.: Characterization and in vitro biological effects of concentrated particulate matter from Mexico City, Atmos. Environ., 40, 583–592, https://doi.org/10.1016/j.atmosenv.2005.12.073, 2006.

Dusek, U., Reischl, G. P., and Hitzenberger, R.: CCN activation of pure and coated carbon black particles, Environ. Sci. Technol., 40, 1223–1230, https://doi.org/10.1021/es0503478, 2006.

Ervens, B., Cubison, M., Andrews, E., Feingold, G., Ogren, J. A., Jimenez, J. L., DeCarlo, P., and Nenes, A.: Prediction of cloud condensation nucleus number concentration using measurements of aerosol size distributions and composition and light scattering enhancement due to humidity, J. Geophys. Res.-Atmos., 112, 1–15, https://doi.org/10.1029/2006JD007426, 2007.

Fierce, L., Riemer, N., and Bond, T. C.: When is cloud condensation nuclei activity sensitive to particle characteristics at emission?, J. Geophys. Res.-Atmos., 118, 13476–13488, https://doi.org/10.1002/2013JD020608, 2013.

Frank, G. P., Dusek, U., and Andreae, M. O.: Technical Note: Characterization of a static thermal-gradient CCN counter, Atmos. Chem. Phys., 7, 3071–3080, https://doi.org/10.5194/acp-7-3071-2007, 2007.

Furutani, H., Dallosto, M., Roberts, G., and Prather, K.: Assessment of the relative importance of atmospheric aging on CCN activity derived from field observations, Atmos. Environ., 42, 3130–3142, https://doi.org/10.1016/j.atmosenv.2007.09.024, 2008.

Geller, M. D., Biswas, S., Fine, P. M., and Sioutas, C.: A new compact aerosol concentrator for use in conjunction with low flow-rate continuous aerosol instrumentation, J. Aerosol Sci., 36, 1006–1022, https://doi.org/10.1016/j.jaerosci.2004.11.015, 2005.

Gerlofs-Nijland, M. E., Totlandsdal, A. I., Kilinç, E., Boere, A. J. F., Fokkens, P. H., Leseman, D. L., Sioutas, C., Schwarze, P. E., Spronk, H. M., Hadoke, P. W., Miller, M. R., and Cassee, F. R.: Pulmonary and cardiovascular effects of traffic-related particulate matter: 4-week exposure of rats to roadside and diesel engine exhaust particles, Inhal. Toxicol., 22, 1162–1173, https://doi.org/10.3109/08958378.2010.531062, 2010.

Giebl, H., Berner, A., Reischl, G., Puxbaum, H., Kasper-Giebl, A., and Hitzenberger, R.: CCN activation of oxalic and malonic acid test aerosols with the University of Vienna cloud condensation nuclei counter, J. Aerosol Sci., 33, 1623–1634, https://doi.org/10.1016/S0021-8502(02)00115-5, 2002.

Henning, S., Rosenørn, T., D'Anna, B., Gola, A. A., Svenningsson, B., and Bilde, M.: Cloud droplet activation and surface tension of mixtures of slightly soluble organics and inorganic salt, Atmos. Chem. Phys., 5, 575–582, https://doi.org/10.5194/acp-5-575-2005, 2005.

Hinds, W. C.: Aerosol technology: Properties, behavior, and measurement of airborne particles, A Wiley-Interscience publication, Wiley, New York, 2. ed. edn., 1999.

Hings, S. S., Wrobel, W. C., Cross, E. S., Worsnop, D. R., Davidovits, P., and Onasch, T. B.: CCN activation experiments with adipic acid: effect of particle phase and adipic acid coatings on soluble and insoluble particles, Atmos. Chem. Phys., 8, 3735–3748, https://doi.org/10.5194/acp-8-3735-2008, 2008.

Hitzenberger, R., Berner, A., Kasper-Giebl, A., Löflund, M., and Puxbaum, H.: Surface tension of Rax cloud water and its relation to the concentration of organic material, J. Geophys. Res.-Atmos., 107, 1–6, https://doi.org/10.1029/2002JD002506, 2002.

Houghton, J.: The science of global warming, Interdiscipl. Sci. Rev., 26, 247–257, https://doi.org/10.1179/030801801679485, 2001.

IPCC: Climate Change 2013: The Physical Science Basis. Contribution of Working Group I to the Fifth Assessment Report of the Intergovernmental Panel on Climate Change, Cambridge University Press, Cambridge, UK and New York, NY, USA, 2013.

Kanakidou, M., Seinfeld, J. H., Pandis, S. N., Barnes, I., Dentener, F. J., Facchini, M. C., Van Dingenen, R., Ervens, B., Nenes, A., Nielsen, C. J., Swietlicki, E., Putaud, J. P., Balkanski, Y., Fuzzi, S., Horth, J., Moortgat, G. K., Winterhalter, R., Myhre, C. E. L., Tsigaridis, K., Vignati, E., Stephanou, E. G., and Wilson, J.: Organic aerosol and global climate modelling: a review, Atmos. Chem. Phys., 5, 1053–1123, https://doi.org/10.5194/acp-5-1053-2005, 2005.

Kim, S., Jaques, P. A., Chang, M., Froines, J., and Sioutas, C.: Versatile concentration enrichment system (VACES) for simultaneous in vivo and in vitro evaluation of toxic effects of ultrafine, fine and course ambient particles. Part I: Development and laboratory characterization, J. Aerosol Sci., 32, 1281–1297, https://doi.org/10.1016/S0021-8502(01)00057-X, 2001a.

Kim, S., Jaques, P. A., Chang, M., Barone, T., Xiong, C., Friedlander, S. K., and Sioutas, C.: Versatile aerosol concentration enrichment system (VACES) for simultaneous in vivo and in vitro evaluation of toxic effects of ultrafine, fine and coarse ambient particles Part II: Field evaluation, J. Aerosol Sci., 32, 1299–1314, https://doi.org/10.1016/S0021-8502(01)00058-1, 2001b.

Klocke, C., Allen, J. L., Sobolewski, M., Mayer-Pröschel, M., Blum, J. L., Lauterstein, D., Zelikoff, J. T., and Cory-Slechta, D. A.: Neuropathological consequences of gestational exposure to concentrated ambient fine and ultrafine particles in the mouse, Toxicol. Sci., 156, 492–508, https://doi.org/10.1093/toxsci/kfx010, 2017.

Kreidenweis, S. M., Petters, M. D., and DeMott, P. J.: Deliquescence-controlled activation of organic aerosols, Geophys. Res. Lett., 33, 1–4, https://doi.org/10.1029/2005GL024863, 2006.

Kulkarni, P., Baron, P. A., and Willeke, K.: Aerosol Measurement: Principles, Techniques, and Applications, John Wiley & Sons, Hoboken, NJ, 3 edn., 2011.

Kulmala, M., Laaksonen, A.,Charlson, R. J., and Korhonen, P.: Clouds without supersaturation, Nature, 388, 336–337, https://doi.org/10.1038/41000, 1997.

Laaksonen, A., Korhonen, P., Kulmala, M., and Charlson, R. J.: Modification of the Köhler Equation to Include Soluble Trace Gases and Slightly Soluble Substances, J. Atmos. Sci., 55, 853–862, 1998.

Ljubimova, J. Y., Braubach, O., Patil, R., Chiechi, A., Tang, J., Galstyan, A., Shatalova, E. S., Kleinman, M. T., Black, K. L., and Holler, E.: Coarse particulate matter (PM2.5-10) in Los Angeles Basin air induces expression of inflammation and cancer biomarkers in rat brains, Sci. Rep., 8, 5708, https://doi.org/10.1038/s41598-018-23885-3, 2018.

Lohmann, U. and Feichter, J.: Global indirect aerosol effects: a review, Atmos. Chem. Phys., 5, 715–737, https://doi.org/10.5194/acp-5-715-2005, 2005.

Loxham, M., Cooper, M. J., Gerlofs-Nijland, M. E., Cassee, F. R., Davies, D. E., Palmer, M. R., and Teagle, D. A.: Physicochemical characterization of airborne particulate matter at a mainline underground railway station, Environ. Sci. Technol., 47, 3614–3622, https://doi.org/10.1021/es304481m, 2013.

Marple, V. A. and Chien, C. M.: Virtual Impactors: A Theoretical Study, Environ. Sci. Technol., 14, 976–985, https://doi.org/10.1021/es60168a019, 1980.

McFiggans, G., Artaxo, P., Baltensperger, U., Coe, H., Facchini, M. C., Feingold, G., Fuzzi, S., Gysel, M., Laaksonen, A., Lohmann, U., Mentel, T. F., Murphy, D. M., O'Dowd, C. D., Snider, J. R., and Weingartner, E.: The effect of physical and chemical aerosol properties on warm cloud droplet activation, Atmos. Chem. Phys., 6, 2593–2649, https://doi.org/10.5194/acp-6-2593-2006, 2006.

Nenes, A., Conant, W. C., and Seinfeld, J. H.: Black carbon radiative heating effects on cloud microphysics and implications for the aerosol indirect effect 2. Cloud microphysics, J. Geophys. Res.-Atmos., 107, AAC 24-1–AAC 24-11, https://doi.org/10.1029/2002JD002101, 2002.

Ning, Z., Moore, K. F., Polidori, A., and Sioutas, C.: Field Validation of the New Miniature Versatile Aerosol Concentration Enrichment System (mVACES), Aerosol Sci. Tech., 40, 1098–1110, https://doi.org/10.1080/02786820600996422, 2006.

Ntziachristos, L., Ning, Z., Geller, M. D., Sheesley, R. J., Schauer, J. J., and Sioutas, C.: Fine, ultrafine and nanoparticle trace element compositions near a major freeway with a high heavy-duty diesel fraction, Atmos. Environ., 41, 5684–5696, https://doi.org/10.1016/j.atmosenv.2007.02.043, 2007.

Okada, K. and Hitzenberger, R. M.: Mixing properties of individual submicrometer aerosol particles in Vienna, Atmos. Environ., 35, 5617–5628, https://doi.org/10.1016/S1352-2310(01)00126-1, 2001.

Pakbin, P., Ning, Z., Eiguren-Fernandez, A., and Sioutas, C.: Modification of the Versatile Aerosol Concentration Enrichment System (VACES) for conducting inhalation exposures to semi-volatile vapor phase pollutants, J. Aerosol Sci., 42, 555–566, https://doi.org/10.1016/j.jaerosci.2011.06.002, 2011.

Plummer, L. E., Ham, W., Kleeman, M. J., Wexler, A., and Pinkerton, K. E.: Part A, 75, 253–271, https://doi.org/10.1080/15287394.2012.640102, 2012.

Pruppacher, H. and Klett, J.: Microphysics of Clouds and Precipitation, Springer Science & Business Media, Berlin, Germany, 2 edn., 2010.

Reade, L., Jennings, S. G., and McSweeney, G.: Cloud condensation nuclei measurements at Mace Head, Ireland, over the period 1994–2002, Atmos. Res., 82, 610–621, https://doi.org/10.1016/j.atmosres.2006.02.017, 2006.

Rose, D., Gunthe, S. S., Mikhailov, E., Frank, G. P., Dusek, U., Andreae, M. O., and Pöschl, U.: Calibration and measurement uncertainties of a continuous-flow cloud condensation nuclei counter (DMT-CCNC): CCN activation of ammonium sulfate and sodium chloride aerosol particles in theory and experiment, Atmos. Chem. Phys., 8, 1153–1179, https://doi.org/10.5194/acp-8-1153-2008, 2008.

Saarikoski, S., Carbone, S., Cubison, M. J., Hillamo, R., Keronen, P., Sioutas, C., Worsnop, D. R., and Jimenez, J. L.: Evaluation of the performance of a particle concentrator for online instrumentation, Atmos. Meas. Tech., 7, 2121–2135, https://doi.org/10.5194/amt-7-2121-2014, 2014.

Seinfeld, J. H. and Pandis, S. N.: Atmospheric Chemistry and Physics: From Air Pollution to Climate Change, John Wiley & Sons, Hoboken, NJ, 2 edn., 2006.

Sioutas, C. and Koutrakis, P.: Inertial separation of ultrafine particles using a condensational growth/virtual impaction system, Aerosol Sci. Tech., 25, 424–436, https://doi.org/10.1080/02786829608965407, 1996.

Sioutas, C., Koutrakis, P., and Olson, B. A.: Development and evaluation of a low cutpoint virtual impactor, Aerosol Sci. Tech., 21, 223–235, https://doi.org/10.1080/02786829408959711, 1994.

Sioutas, C., Kim, S., and Chang, M.: Development and evaluation of a prototype ultrafine particle concentrator, J. Aerosol Sci., 30, 1001–1017, https://doi.org/10.1016/S0021-8502(98)00769-1, 1999.

Steenhof, M., Gosens, I., Strak, M., Godri, K. J., Hoek, G., Cassee, F. R., Mudway, I. S., Kelly, F. J., Harrison, R. M., Lebret, E., Brunekreef, B., Janssen, N. A. H., and Pieters, R. H. H.: In vitro

toxicity of particulate matter (PM) collected at different sites in the Netherlands is associated with PM composition, size fraction and oxidative potential – the RAPTES project, Part. Fibre Toxicol., 8, 1–15, https://doi.org/10.1186/1743-8977-8-26, 2011.

Tomasi, C., Fuzzi, S., and Kochanovskij, A. A.: Atmospheric aerosols: Life cycles and effects on air quality and climate, Wiley series in atmospheric physics and remote sensing, Wiley-VCH, Weinheim, 2017.

Twomey, S.: The Influence of Pollution on the Shortwave Albedo of Clouds, J. Atmos. Sci., 34, 1149–1152, 1977.

Tzamkiozis, T., Stoeger, T., Cheung, K., Ntziachristos, L., Sioutas, C., and Samaras, Z.: Monitoring the inflammatory potential of exhaust particles from passenger cars in mice, Inhal. Toxicol., 22, 59–69, https://doi.org/10.3109/08958378.2010.519408, 2010.

Verma, V., Pakbin, P., Cheung, K. L., Cho, A. K., Schauer, J. J., Shafer, M. M., Kleinman, M. T., and Sioutas, C.: Physicochemical and oxidative characteristics of semi-volatile components of quasi-ultrafine particles in an urban atmosphere, Atmos. Environ., 45, 1025–1033, https://doi.org/10.1016/j.atmosenv.2010.10.044, 2011.

Wang, D., Kam, W., Cheung, K., Pakbin, P., and Sioutas, C.: Development of a two-stage virtual impactor system for high concentration enrichment of ultrafine, pm2.5, and coarse particulate matter, Aerosol Sci. Tech., 47, 231–238, https://doi.org/10.1080/02786826.2012.744446, 2013a.

Wang, D., Pakbin, P., Saffari, A., Shafer, M. M., Schauer, J. J., and Sioutas, C.: Development and evaluation of a high-volume aerosol-into-liquid collector for fine and ultrafine particulate matter, Aerosol Sci. Tech., 47, 1226–1238, https://doi.org/10.1080/02786826.2013.830693, 2013b.

Wang, D., Pakbin, P., Shafer, M. M., Antkiewicz, D., Schauer, J. J., and Sioutas, C.: Macrophage reactive oxygen species activity of water-soluble and water-insoluble fractions of ambient coarse, PM2.5 and ultrafine particulate matter (PM) in Los Angeles, Atmos. Environ., 77, 301–310, https://doi.org/10.1016/J.ATMOSENV.2013.05.031, 2013c.

Wang, D., Sowlat, M. H., Shafer, M. M., Schauer, J. J., and Sioutas, C.: Development and evaluation of a novel monitor for on-line measurement of iron, manganese, and chromium in ambient particulate matter (PM), Sci. Total Environ., 565, 123–131, https://doi.org/10.1016/j.scitotenv.2016.04.164, 2016.

Wang, W., Zhou, J., Chen, M., Huang, X., Xie, X., Li, W., Cao, Q., Kan, H., Xu, Y., and Ying, Z.: Exposure to concentrated ambient PM 2.5 alters the composition of gut microbiota in a murine model, 15, https://doi.org/10.1186/s12989-018-0252-6, 2018.

Weast, R. C.: CRC handbook of chemistry and physics, Boca Raton, FL, crc press edn., 1988.

Winklmayr, W., Reischl, G., Lindner, A., and Berner, A.: A new electromobility spectrometer for the measurement of aerosol size distributions in the size range from 1 to 1000 nm, J. Aerosol Sci., 22, 289–296, https://doi.org/10.1016/S0021-8502(05)80007-2, 1991.

Zhang, Q., Meng, J., Quan, J., Gao, Y., Zhao, D., Chen, P., and He, H.: Impact of aerosol composition on cloud condensation nuclei activity, Atmos. Chem. Phys., 12, 3783–3790, https://doi.org/10.5194/acp-12-3783-2012, 2012.

Zhao, Y., Bein, K., Wexler, A., Misra, C., Fine, P., and C. Sioutas, C.: Field evaluation of the versatile aerosol concentration enrichment system (VACES) particle concentrator coupled to the rapid single-particle mass spectrometer (RSMS-3), J. Geophys. Res., 110, D07S02, https://doi.org/10.1029/2004JD004644, 2005.